Analysis and Design of an Omnidirectional Platform for Operation on Non-Ideal Floors

Matthew Spenko Haoyong Yu Steven Dubowsky
Department of Mechanical Engineering
Massachusetts Institute of Technology
Cambridge, MA 02139 USA

Abstract

An omnidirectional platform with an Active Offset Split Caster (ASOC) is described and its ability to operate on non-ideal floors is studied. It is shown that all of its driven wheels of the platform will remain in contact with an uneven floor at all times, a condition necessary to maintain good traction and dead-reckoning capabilities. It is shown that planning algorithms developed for an ideally flat floor perform adequately for a realistic uneven floor. Furthermore, it is shown that the ASOC design consumes less power than other conventional wheel omnidirectional designs and is more suitable to heavier loads. Analytical and experimental results are presented.

1 Introduction

Mobile robotic vehicles built on Omnidirectional Mobility Platforms (OMP) have advantages over non-omnidirectional platforms in congested environments such as factories, eldercare facilities, and hospitals (West and Asada, 1997).

The performance of OMPs can be degraded when operating on realistic floors. Dirt and debris, wires, gaps, bumps at the joints between tile and carpet, and unevenness can reduce dead-reckoning and traction as well as increasing power consumption when heavily loaded. These problems are addressed here for an OMP using split caster wheel designs.

Most OMPs fall into two categories: those with special wheels and those that use conventional wheels. Special wheel designs can produce good omni-directional mobility, but they are generally costly, complex, and sensitive to debris and vibrations (Fujisawa, '97; Ferriere, '98; Muir, '87; Killough, '94; West, '97). In contrast, OMPs that use conventional wheels are generally mechanically simple and have smooth action. The most common OMP designs using conventional wheels steer the wheels by twisting them around an axis perpendicular to the floor (see Figure 1) (Boreinstein, et al., '96; Wada, '96; Holmberg, '99). One drawback of these actively-steered designs is that as the wheel is twisted, it experiences high scrubbing forces (Killough, '94). This reduces positioning accuracy and increases power consumption and tire wear. A dual wheel design similar to that found in aircraft landing gear can mitigate these problems (Wada, 2000; Yu, 2000). A form of this design is called the Active Split Offset Caster (ASOC), which has two independently driven wheels separated by link labeled the "split" and offset from a shaft that it is free to rotate about (see Figure 1 and Figure 2) (Yu, 2000). The OMP shown uses two ASOC's and two passive casters. This design has been implemented on an intelligent mobility aid for the elderly called the SmartWalker and has been found to be very effective for the application (see Figure 3) (Dubowsky, 2000).

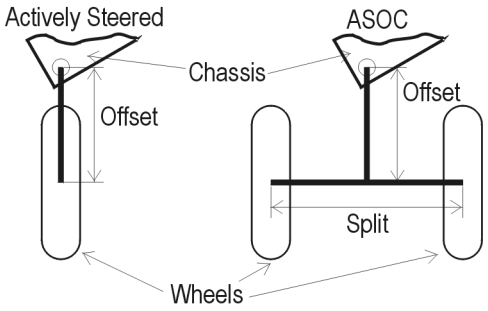

Figure 1: Actively Steered Caster and ASOC

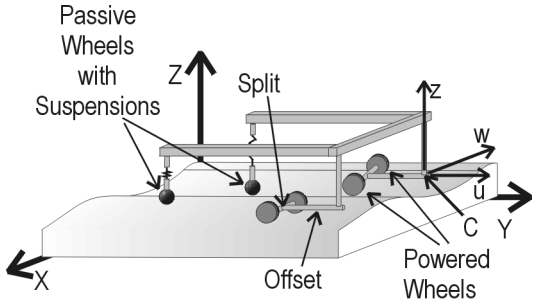

Figure 2: OMP on Inertial Reference Frame

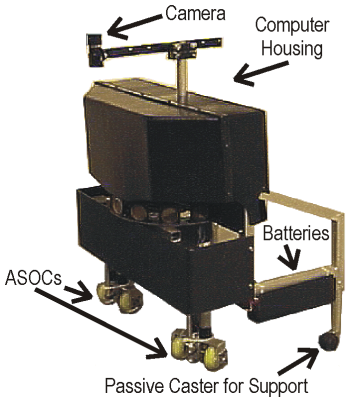

Figure 3: The SmartWalker with Its OMP

In this paper, the performance of this design on realistic uneven floors is explored. It is shown that with a passive DOF added to the ASOCs, all the wheels of the OMP will remain in contact with an uneven floor at all times. This is required to ensure good traction. It is further shown that the addition of the passive joint does not significantly affect the dead reckoning accuracy of the platform on non-ideal uneven floors. Finally, it is shown that this design has smaller power consumption than other OMPs with conventional wheel designs.

2 ASOC Contact on Uneven Floors

Some designs will lose contact with an uneven floor and fail to function properly (Wada, 2000). This is obvious for the simple planar case shown in Figure 4.

Figure 4: Loss of Contact on an Uneven Floor

To overcome this problem, a passive pivot joint has been added at point C to the ASOC design. This allows the wheel pair to rotate freely about the **u**-axis (see Figure 5).

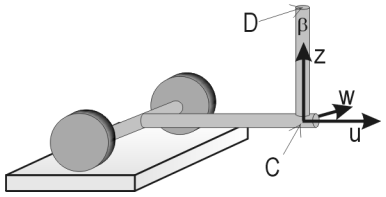

Figure 5: Notation of Various Points on the ASOC

However, two questions remain. First, is contact with the ground rigorously guaranteed at all times? Second, does the system with the added joints have sufficient dead reckoning capabilities on uneven floors?

The analysis shows that all of the wheels can touch the ground at the same time by first showing that the two wheels of one ASOC touch the ground, then by showing that the workspace of the second ASOC's wheels can lie on the ground, and then finally by showing that any of the passive casters can touch the ground if they have proper independent suspensions.

Assume that the wheels are modeled as thin disks, then given a point on the ground, $P_1(x_1,y_1,z_1)$, then referring to Figure 6, a second point, $P_2(x_2,y_1,z_2)$, is chosen to lie in the same plane, $\mathcal{P}_{XZ}$, as P_1 with the constraint that:

$$d = \sqrt{(x_2 - x_1)^2 + (z_2 - z_1)^2} \qquad (1)$$

where d is the length between the two wheels.

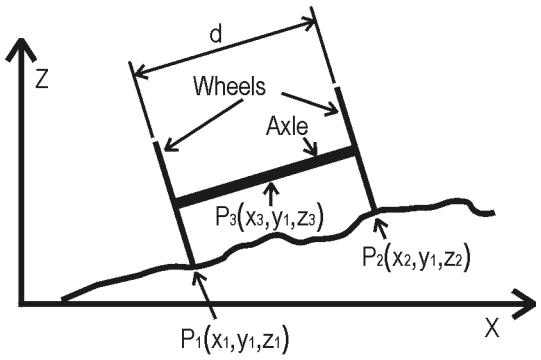

Figure 6: ASOC on Uneven Terrain

The ground can be can be represented by z=f(x). So, given x_1, it is possible to find z_1. Knowing x_1 and z_1 and utilizing Equation 1, it is possible to determine the location of point P_2. Assuming that the axle also lies in the XZ plane, it is possible to locate the point $P_3(x_3,y_1,z_3)$, which is the location of the joint in the ASOC.

Then by geometry, the point C is found by translating the point P_3 along Y-axis by a distance s (see Figure 7). It can be shown that from point C the workspace of the point $P_3'(x_3',y_3',z_3')$, the point on the second ASOC corresponding to P_3, is bounded by the inequality:

$$(h-s)^2 \le (x_3' - x_3)^2 + (y_3' - (y_1 + s))^2 + (z_3' - z_3)^2 \le (h+s)^2 \quad (2)$$

where h is the length of the bar that attaches the ASOCs.

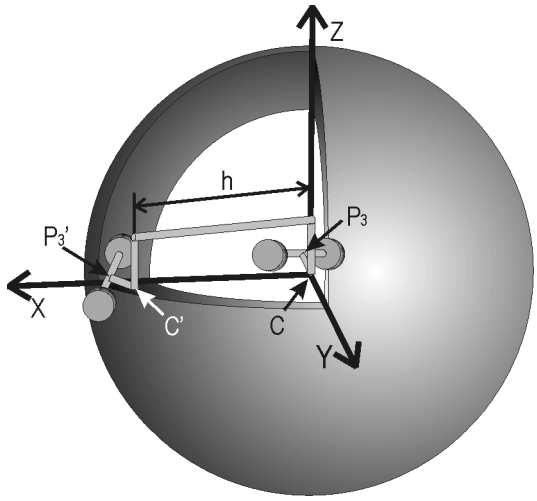

Figure 7: Workspace of the Second ASOC

This can be compared to the workspace of a platform had it not contained any joints, which is defined by the following inequality (see Figure 8):

$$(h-s)^2 \le (x_3' - x_3)^2 + (y_3' - (y_1' + s))^2 \le (h+s)^2 \qquad (3)$$

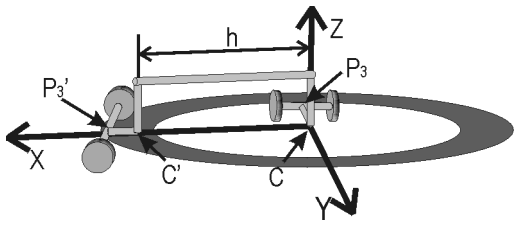

Figure 8: Workspace of Second ASOC without Added Joint

For the case with the joint, as long as the terrain exists inside of the configuration space, which is true for all cases except when the terrain is a sphere with a radius less than (h + s), then the point P_3' can exist at any height above the terrain. If that is the case, then the two points P_1' and P_2' can also exist. This is possible because given P_1, it is possible to find P_2 and P_3. Applying the converse, given P_3' it is possible to find P_1' and P_2'. Thus, all four wheels of the two ASOCs can touch the ground at the same time on an uneven terrain, and designs that do not employ this passive joint will suffer if used on uneven floors.

The passive casters will contact the ground as long as they have a suspension that allows them to elongate linearly downward and the ground lies within the allowable travel of the suspension. Thus, all of the wheels of the OMP touch the ground at all times

2.1 Dead-Reckoning Accuracy on Uneven Floors

Here, the equation that describes the velocity of one ASOC traversing an uneven floor in three dimensions is derived. Simulations are presented that show that an ASOC running over a bump in the floor will not significantly deviate from the desired path even when the wheel velocities are determined using a flat floor planning model (Yu, 2000). The base plane, $\mathscr{P}_{\text{base}}$, is considered to be the "flat floor" and is defined by z=0, where the gravity vector $\mathbf{n} = [0,0,-1]^T$ is normal to $\mathscr{P}_{\text{base}}$. The encoder shaft (the shaft between points C and D in Figure 5) of the ASOC is assumed to always be normal to $\mathscr{P}_{\text{base}}$. This ensures that $\mathbf{n}_{EncoderShaft}=[0,0,1]^T$. This statement does not hold true for exceptionally rough surfaces, but is valid for this case of slightly uneven floors.

Other dimensions that must be defined are the angle θ, which is the amount that the ASOC is tilted about the u-axis, and angles γ_1 and γ_2, which are the contact angles of the ground at each wheel respectively. The dimension s is the length of the offset and d is the length of the split, and Ψ is the angle of the ASOC with respect to the X-axis (see Figure 9).

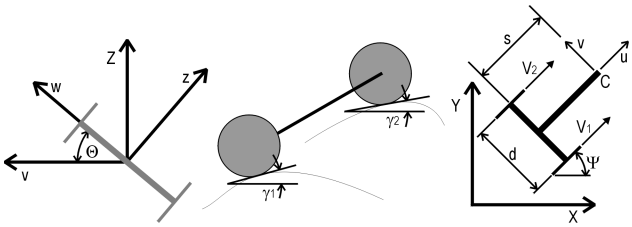

Figure 9: Explanation of Various Dimensions

The velocity of point C in the inertial reference frame (the ground) for the two-dimensional case is given as (Yu, 2000):

$$\begin{bmatrix} V_X \\ V_Y \end{bmatrix} = \begin{bmatrix} \frac{1}{2}(V_1+V_2)\cos\Psi - \frac{s(\sin\Psi)}{d}(V_1-V_2) \\ \frac{1}{2}(V_1+V_2)\sin\Psi + \frac{s(\cos\Psi)}{d}(V_1-V_2) \end{bmatrix} \tag{4}$$

For the three-dimensional case, the velocity of point D needs to be determined (see Figure 5) and is given by:

$${}_{\alpha}\mathbf{v}_{D/O} = {}_{\alpha}\mathbf{v}_{D/C} + {}_{\alpha}\mathbf{v}_{C/O} \tag{5}$$

where the α-frame is the inertial frame. For a given V_1 and V_2, the respective velocities of each of the wheels, the velocity of point C in the three-dimensional case is:

$$\begin{aligned} {}_{\alpha}\mathbf{V}_{C/O} = &\left(\frac{1}{2}(V_1\cos\gamma_1 + V_2\cos\gamma_2)\right)\mathbf{u} + \left(\frac{s}{d}(V_1-V_2)\right)\mathbf{w} + \\ &\left(\frac{1}{2}(V_1\sin\gamma_1 + V_2\sin\gamma_2)\right)\mathbf{z} \end{aligned} \tag{6}$$

As the floor becomes uneven, the joint rotates an angle of θ and with an angular velocity of $\dot{\theta}$. Thus:

$${}_{\alpha}\mathbf{v}_{D/C} = \left[-\dot{\Theta}l\cos\Theta\right]\mathbf{w} - \left[\dot{\Theta}l\sin\Theta\right]\mathbf{z} \tag{7}$$

where l is the distance between points C and D. Thus:

$$\begin{aligned} {}_{\alpha}\mathbf{V}_{D} = &\left(\frac{1}{2}(V_1\cos\gamma_1 + V_2\cos\gamma_2)\right)\mathbf{u} + \left(\frac{s}{d}(V_1-V_2) - \dot{\Theta}l\cos\Theta\right)\mathbf{w} + \\ &\left(\left(\frac{1}{2}(V_1\cos\gamma_1 + V_2\cos\gamma_2)\right) - \left(\dot{\Theta}l\sin\Theta\right)\right)\mathbf{z} \end{aligned} \tag{8}$$

After a coordinate transformation in accordance with Euler's Angles, the velocity of point D is given as:

$$\begin{bmatrix} V_X \\ V_Y \\ V_Z \end{bmatrix} = \begin{bmatrix} \frac{1}{2}(V_1\cos\gamma_1+V_2\cos\gamma_2)\cos\Psi + \sin\Psi\begin{pmatrix} \dot{\Theta}l\left(\cos^2\Theta-\sin^2\Theta\right)\frac{s}{d}+ \\ \frac{1}{2}(V_1\sin\gamma_1+V_2\sin\gamma_2)\sin\Theta \\ -\frac{s}{d}\cos\Theta(V_1-V_2) \end{pmatrix} \\ \frac{1}{2}(V_1\cos\gamma_1+V_2\cos\gamma_2)\sin\Psi - \cos\Psi\begin{pmatrix} \dot{\Theta}l\left(\cos^2\Theta-\sin^2\Theta\right)\frac{s}{d}+ \\ \frac{1}{2}(V_1\sin\gamma_1+V_2\sin\gamma_2)\sin\Theta \\ -\frac{s}{d}\cos\Theta(V_1-V_2) \end{pmatrix} \\ \frac{1}{2}(V_1\sin\gamma_1+V_2\sin\gamma_2)\cos\Theta + \sin\Theta\left(\frac{s}{d}(V_1-V_2) - 2\dot{\Theta}l\cos\Theta\right) \end{bmatrix} \tag{9}$$

It can be shown that for θ, γ, and $\dot{\theta}$ equal to zero, Equation 9 simplifies to the equation that was derived for the flat ground (see Equation 4).

To evaluate the system tracking or dead-reckoning performance on an uneven floor, a simulation of an ASOC running over a bump in the floor was done. The bump was modeled by the function:

$$z = (amp)e^{-(peak*x)^2-(peak*y)^2} \tag{10}$$

where *amp* is the height of the bump in meters and *peak* is the sharpness of the bump (units length^{-1}). The simulation uses the same dimensions as the found in the SmartWalker (Dubowsky, 2000). The deviation of point D from the desired path was found for bump sizes ranging from 0 to 40 mm with a peak value of 15. The results show that point D only deviates from its intended path by approximately the height of the bump. Most indoor floors used by the SmartWalker would be in the range of 0 to 3 mm with a possible maximum height of 10 mm.

A simulation of the OMP traversing uneven terrain is also done. The terrain is defined by the function:

$$z = amp\left(x^3 - \frac{(1-x)^2}{3} - \frac{x}{5} + y^5\right)e^{-x^2-y^2} \tag{11}$$

The results show that after traveling over 14 m, the OMP returns to within 4mm of its starting position (see Figure 10). This is difficult to resolve from the figure, but it also indicates that the planning algorithm is acceptable for an uneven floor.

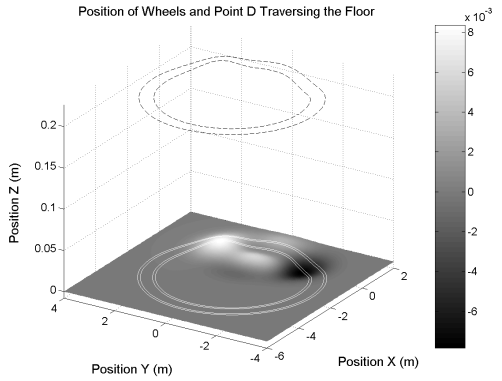

Figure 10: Position of Wheels and Point D of the OMP Traversing Uneven Terrain

It should be noted that a number of other factors such as wheel compression under load and structural misalignment will affect a platform's open-loop control accuracy. However, the more accurate a platform is, the less errors a closed-loop control system needs to compensate for. In the case of the SmartWalker, this means that the vision system used for closed-loop control can be run less often which in turn frees up valuable computation time.

3 Wheel Scrubbing Analysis

In this section, the power consumption due to scrubbing torque of the ASOC and a conventional actively steered caster are compared. It is shown that the ASOC design uses less power, which makes it better suited for carpeted and other non-ideal surfaces.

Conventional wheels in general motion on a plane experience three main resistance forces: the contact friction f, the rolling resistance M_r, and the scrubbing torque M_s. The scrubbing torque is the torque required to twist a simple single wheel around its vertical axis. For the case of a firm wheel on a rigid floor, such as tile or in the worst case institutional low pile carpet, the scrubbing torque is the dominant force. The scrubbing torque can be calculated by integrating the frictional force elements over the entire contact patch between the wheel and the floor. To do this, the contact pressure distribution is calculated by treating the contact between a solid rubber wheel and a rigid floor as a Hertzian contact problem where the normal pressure is multiplied by a coefficient of friction to yield the local shear stress (Slocum, 1992). Integrating the torque due to the shear stress over the contact area yields the scrubbing torque. For a cylindrical wheel, the scrubbing torque is:

$$M_s = 4\mu\int_0^{B/2}\int_0^b \sqrt{x^2+y^2}\,p(x)dxdy \tag{12}$$

where p(x) is the Hertzian pressure distribution and can be easily estimated (Barber, 1992). Other dimensions are shown in Figure 11. This equation can be solved with numerical methods.

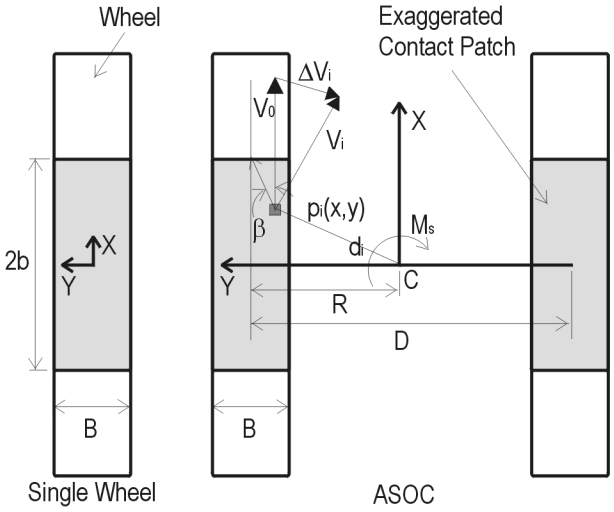

Figure 11: Scrubbing Analysis for Notation for Single Wheel and ASOC Design

Now consider a dual wheel pair separated at a distance of D (see Figure 11). Under the same total load, each of the two wheels has a contact area similar in shape to the single wheel case, but the contact pressure is lower. When the wheel set is twisted around its center for a full turn, the contact patches of the two wheels also undergo a full rotation. For a single wheel twisted around its vertical axis under the twisting moment T, there is no initial relative motion between the wheel material and the floor. Instead, the material deforms in the tangential direction. As T increases, this deformation reaches a limit and slippage (or scrubbing) occurs.

For the dual wheel case, when the wheel set is twisted around its center at an angular velocity ω_s, both of its wheels are rolling at a speed of $(D*\omega_s)/2$. The actual velocities at various points in the contact area are different. Therefore, on the outer edge of the wheel, the wheel material is being stretched and on the inner edge of the wheel, the material is being compressed. At those points with velocity difference, deformation happens as the material elements make contact with the floor. The tangential deformation of a element $p_i(x,y)$ (see Figure 11) within the contact patch can be expressed as the ratio of the velocity difference over the rolling velocity, V_0, of the wheel, which is given as:

$$\varepsilon_i = \frac{\|\Delta V_i\|}{\|V_0\|} = \frac{\|\vec{d}_i - \vec{R}\|}{R} \qquad (13)$$

where d_i is the distance from the center, C. If ε_i does not reach a limit ε_0, which is determined experimentally, that element is not considered when determining the scrubbing torque. However, if ε_i does reach a limit ε_0, the scrubbing torque of that element is given as:

$$\Delta M_s = \mu p(x,y) \cdot (x \sin\beta - y \cos\beta) dxdy \qquad (14)$$

If these elements are integrated over the entire contact patch, the scrubbing torque of the wheel is given. In the single wheel case, ε_i at every point in the contact patch will eventually reach a limit, ε_0, and slippage will occur. In the dual wheel case, at those points where ε_i is small, no slippage will occur before the wheel rolls over to the next element, resulting in no contribution to the scrubbing torque. Therefore, wheel scrubbing happens in the dual wheel design; however, it is less than in the single wheel case. From Equation (12), it also can be seen that ε_i does not depend on the wheel speed, only the separation distance.

The scrubbing power for the ASOC and active steered caster are compared. In each case, the caster is commanded to drive the chassis in a straight line to the right (see Figure 12).

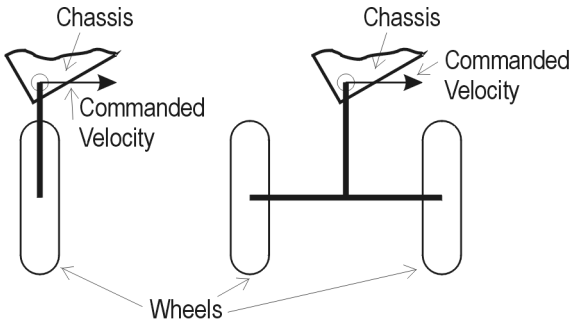

Figure 12: Commanded Path

The simulation results (see Figure 13) show that the active castor has a higher scrubbing torque and higher total power consumption than the ASOC.

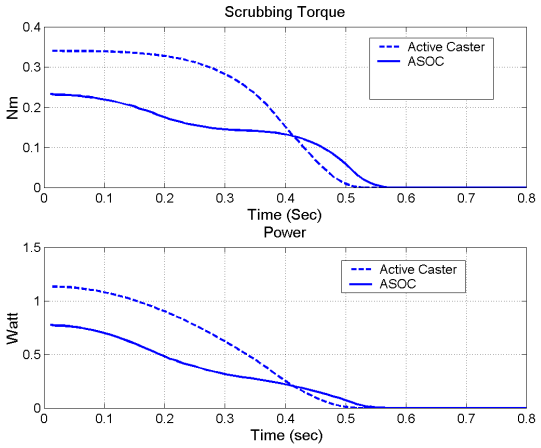

Figure 13: Scrubbing Comparison of ASOC and Active Caster

In addition, the scrubbing torque is a function of the distance between the two wheels. Figure 14 shows this effect, where the different values of ε_0 show the effect of the elasticity between the floor and the wheel.

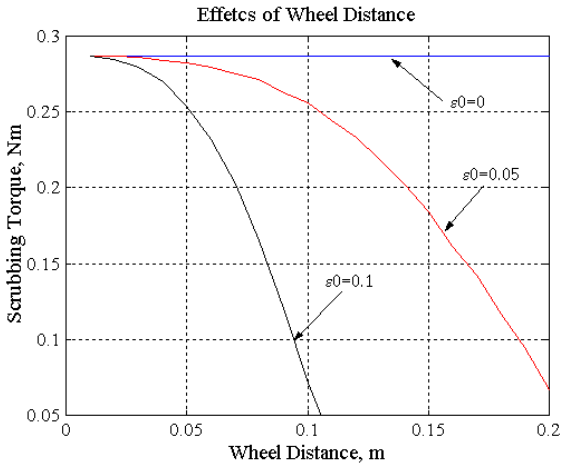

Figure 14: Effect of Wheel Distance on Scrubbing Torque

The figure shows that as the distance between the wheels is increased, the scrubbing torque decreases. It also shows that a more elastic material will contribute less scrubbing torque.

4 Experiments

To demonstrate and evaluate the effectiveness of the ASOC, a series of experiments were performed using different paths which included circular, rectangular, and combined translational and rotational motions. The platform demonstrated smooth motion and achieved good tracking performance under open loop control, even for complex trajectories. During the experiments, the actual position and orientation of the system are obtained using the vision based localization system of the SmartWalker (Dubowsky, 2000).

The walker is commanded to follow a trajectory that is about 15 meters long with several sharp turns (see Figure 15). It travels at a constant speed of 50 cm/s (the speed is limited by the vision system) and does not stop at the turns. The maximum deviation from the path is less than 30 cm. It can be seen that the error results from the angular error when the walker makes a sharp turn over a part of the floor that changed from concrete to a waffle iron plate (point A in Figure 15). Under closed loop control, the trajectory error is reduced to less than 10 cm.

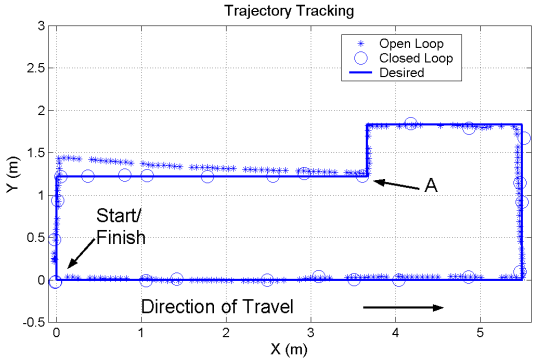

Figure 15: Open vs. Closed Loop Trajectory Tracking

5 Conclusions

It was shown that for conventional wheel designed OMPs, the ASOC design has greater power conservation than an actively steered caster design. It was also shown that a passive joint will allow all of the wheels of the ASOC to maintain contact with a realistic floor. It was further shown that the added suspension does not significantly affect open-loop accuracy of the platform, even when the planning algorithms for a flat floor are used.

6 Acknowledgments

This work is sponsored by the Home Automation and Healthcare Consortium in the MIT d'Arbeloff Laboratory for Information Systems and Technology.

7 References

Barber J. R., *Elasticity*. Kluwer Academic, Netherlands, 1992.

Dubowsky S., et al., "PAMM - A Robotic Aid to the Elderly for Mobility Assistance and Monitoring: A Helping-Hand for the Elderly," *Proc. of IEEE ICRA* 2000.

Ferriere L., Raucent B., "ROLLMOBS, a New Universal Wheel Concept," *Proc. of IEEE ICRA*, Leuven, Belgium, pp.1877-1882, May 1998.

Fujisawa S., et al., "Improved Moving Properties of an Omnidirectional Vehicle Using Stepping Motor," *Proc. of the 36th Conference on Decision & Control*. San Diego, CA, pp.3654-3657, Dec. 1997.

Holmberg R., Khatib O., "Development of a Holonomic Mobile Robot for Mobile Manipulation Tasks," *Proc. Int. Conf. on Field and Service Robotics* Pittsburgh, PA, pp. 268-273, Aug. 1999.

Killough S.M., Pin F.G., "A New Family of Omnidirectional and Holonomic wheeled platforms for mobile robots," *IEEE Transactions on Robotics and Automation*, Vol.10, No.4, pp. 480-489, 1994.

Muir P.F., Neuman C.P., "Kinematic Modeling for Feedback Control of an Omni-directional Wheeled Mobile Robot," *Proc. of IEEE ICRA*, 1987.

Slocum A., *Precision Machine Design.* Prentice Hall, Englewood Cliffs, New Jersey, 1992.

Sreenivasan, S.V., Nanua, P., "Kinematic Geometry of Wheeled Vehicle Systems," *Proc. ASME Design Engineering Technical Conferences and Computers in Engineering*, Irving, CA, August 18-22, 1996.

Wada M., Mori S., "Holonomic and Omnidirectional Vehicle with Conventional Tires," Proceedings of *IEEE ICRA* MN, pp. 3671-3676, April 1996.

Wada M., Takagi, A, Mori, S. "Caster Drive Mechanisms for Holonomic and Omnidirectional Mobile Platforms with No Over Constraint." *Proc. IEEE ICRA* San Francisco, CA, April 2000.

West M., Asada H., "Design of Ball wheel Mechanisms for Omnidirectional Vehicles with Full Mobility and Invariant Kinematics," *Journal of Mechanical Design*, Vol.119, pp153-161, June 1997.

Yu, H., Dubowsky, S., and Skwersky, A., "Omni-directional Mobility Using Active Split Offset Castors," *Proc. of 2000 ASME IDETC/CIE 26th Biennial Mechanics and Robotics Conference* Baltimore, MD, Sept. 2000.